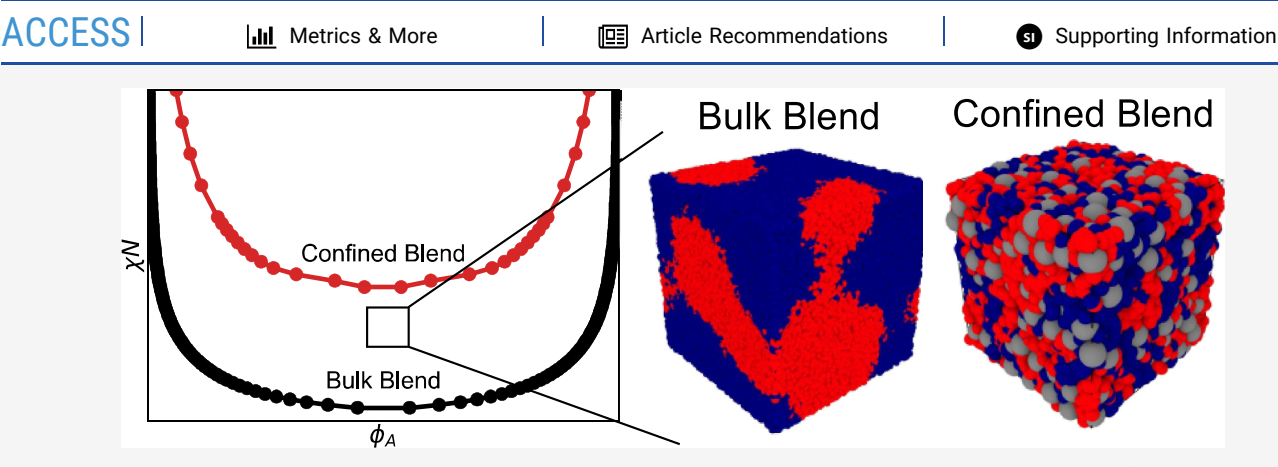


pubs.acs.org/Macromolecules Article

Increases in Miscibility of a Binary Polymer Blend Confined within a Nanoparticle Packing

Anastasia Neuman, Shannon Zhang, Daeyeon Lee,* and Robert A. Riggleman*





ABSTRACT: Despite various physical and chemical strategies that have been explored, compatibilization of polymer blends has proved elusive. Confinement of polymers has shown to induce substantial and at times unexpected changes in glass-transition temperature, dynamics, and morphology of these materials. Although confinement of blends to thin films have shown to influence phase separation structure and chain mobility, the impact of confinement on the miscibility of polymer mixtures is much less understood. Here, we present a computational study using field-theoretic simulations to understand the thermodynamics of polymer blends that are confined in the interstices of nanoparticle packings where both polymers have neutral interactions with the nanoparticle surfaces. We calculate their binodal phase envelopes and show that two polymers that would undergo macroscopic phase separation become miscible when they are subjected to extreme nanoconfinement. The strength of the repulsion required to induce phase separation increases significantly as confinement increases. We find that this enhanced miscibility is driven by both an increase in entropic penalty upon phase separation and a decrease in enthalpic repulsion with increasing confinement. We relate the change in enthalpy to a reduction in the number of polymer—polymer contacts near nanoparticle surfaces and the change in entropy to a reduction in conformational freedom due to the formation of a polymer—polymer interface near nanoparticle surfaces. Confinement-induced mixing of polymers in nanoparticle packings could enable precise tuning of mechanical and transport properties of nanocomposite films and membranes.

B lending two polymers with complementary properties is a versatile method of producing polymer-based materials with tunable properties. However, most polymer blends are immiscible due to their relatively small entropy of mixing and high interfacial tension. The compatibilization of such immiscible blends to achieve improved properties has been an active area of research for many years. A common method involves the addition of a copolymer composed of the two polymers in the blend. A variety of copolymer architectures have been applied for this purpose, including diblock, triblock, branched random or comb, 2 tapered, and grafted 3 polymers. In reactive blending, copolymers are formed in situ via a chemical reaction.^{4,5} Reactive blending is heavily dependent on reaction conditions, with flow in melt mixers impacting interfacial reaction kinetics.⁶ The efficacy of copolymers as compatibilizers, whether added directly to a blend or formed through reactions, is measured by the reduction of interfacial tension,

with the copolymer localizing to the interface between phases and reducing the size of phase-separated domains. The extent of interfacial adsorption by copolymer and thus the decrease in interfacial tension, is limited by micellization; above the critical micelle concentration of the compatibilizer, copolymers form micelles, preventing any further increase in interfacial coverage. Polymer-grafted nanoparticles have also shown promise as compatibilizers through a mechanism similar to copolymers, reducing domain sizes upon phase separation by localizing to

Received: September 15, 2022 Revised: December 23, 2022 Published: January 18, 2023





and reinforcing the interface. ^{9,10} One possibility that has not been extensively explored in enhancing the miscibility of polymer blends is physical confinement. Confining polymers in spaces smaller than their intrinsic size has been shown to induce numerous deviations from their bulk properties including the glass-transition temperature ^{11–14} ($T_{\rm g}$), viscosity, ^{15–18} physical aging rate, ^{19–21} and chain conformation. ^{22–25} It has also been shown that the self-assembly of block copolymers ^{26–28} and crystallization of polymers ^{29,30} can be significantly affected by physical confinement.

Polymer blends under thin film confinement exhibit phase behavior distinct from that of unconfined blends. 31,32 Confinement within nanoporous materials such as periodic gels³³ or metal-organic frameworks³⁴ impacts the phase behavior of near-critical fluids. Simulations based on the Cahn-Hilliard-Cook model have shown that the addition of particles such as spheres, fibers, or platelets induces concentration waves near particle surfaces in near-critical blends when one polymer preferentially wets the particle surface, altering the kinetics and morphology of phase separation.^{35,36} Similar to the compatibilization mechanism of copolymers, a small amount of mobile particles with preferential wetting for one component of the blend reduces the size of phase-separated domains, arresting late stage phase separation.³⁷ The steady-state domain size of such a system depends on the particle concentration and particle diffusion constant, with particles wet by one phase inhibiting coarsening.^{38–41} The particle shape, size, and surface chemistry also impact the nanoparticle localization and thus the final morphology of blends. 42 In studies demonstrating these effects, the changes in phase behavior are primarily enthalpically driven, occurring due to surface interactions and adsorption. The volume fraction of particles in such systems is low (<0.10), leading to a low surface area to polymer volume ratio. Entropic changes due to surfaces have a small correlation length and these effects would not have large impacts on bulk behavior if there is a large bulk volume and low surface area. Only strong surface interactions impact polymer behavior far from surfaces. 33,43,44 DPD simulations that vary the radius of preferentially wetting particles at constant volume fraction (~20%) found that domain growth reduces with decreasing radius or with an increasing nanoparticle surface area to volume ratio. 45 Similar thermodynamic analyses of low volume fraction (<0.20) mobile nanoparticles in a polymer blend also found that miscibility increases with decreasing filler radius.⁴⁶ These studies of ternary polymer-polymer-nanoparticle composite thermodynamics, however, have not addressed the effects of extreme nanoconfinement, due to both the small volume fraction of particles and particle mobility. The effect of physical confinement in the absence of surface interactions or particle mobility has yet to be explored but is of particular interest in a system with a very high loading fraction of particles in a close-packed geometry, where surface entropic effects may impact the entire volume.

Polymer nanocomposites with high volume fractions of nanoparticles present a unique opportunity to study the effect of confinement on polymers while enabling the fabrication of functional materials with useful mechanical, transport, and catalytic properties. Recently, several methods to create highly loaded polymer nanocomposites have been developed, including infiltrating polymers into the nanoparticle packing using thermal annealing via capillary rise infiltration (CaRI), shear pressing, vacuum infiltration, is in situ electropolymerization, and initiated chemical vapor deposi-

tion. 54 The CaRI system is of particular interest, as this method produces composites where the nanoparticle loading approaches random-close packing and the characteristic size of the polymer chain can be much greater than the characteristic pore size in the nanoparticle packing. This creates a unique system to study the behavior of polymers under strong nanoconfinement. CaRI also facilitates the manufacturing of polymer blend composites, introducing an experimental system to explore the thermodynamics of confined polymer blends. 55 Determining the phase diagrams of polymer blends in the interstices of nanoparticle packings, however, can prove challenging due to the range of length scales involved; the average pore size of nanoparticle packings is approximately 30% of the size of nanoparticles. While atomistic models such as molecular dynamics or Monte Carlo simulations capture behavior on relatively small length scales, they fail to capture the larger scale phase behavior of polymer blends.

In this study, we use both a hybrid particle-field (HPF)⁵⁶ implementation of self-consistent field theory (SCFT) and theoretically informed Langevin dynamics (TILD)^{57,58} to investigate the miscibility of polymer blends under confinement within the pores of dense nanoparticle packings. Polymer field theory has been an essential tool for calculating polymeric phase diagrams for systems spanning multiple length scales, and under the mean-field approximation allows for the direct calculation of the free energy and phase boundaries.⁵⁹ Several strategies for incorporating nanoparticles into polymer field theory have emerged, 56,60,61 though most work has been primarily focused on the limit of lower nanoparticle concentrations. We find that the nanoconfinement present in highly filled nanocomposites can induce miscibility in incompatible polymer blends, and much stronger polymerpolymer repulsions are required to induce phase separation as the extent of nanoconfinement is increased. The thermodynamic origins for the observed miscibility are investigated. Previous studies have demonstrated increases in miscibility for polymer blends confined to thin films between two walls, in the case of symmetric preferential wetting of one polymer, asymmetric wetting of either polymer by one of the two walls, and homogeneously wetting walls. 62-65 In thin films, polymers are subjected to 1D confinement, where confinement exists only in the direction perpendicular to the surfaces and the polymers have freedom to stretch in the other two directions. Here, we explore a polymer blend undergoing 3D confinement within a network of densely packed spheres. The length scale of confinement described in this work is much smaller than previous studies on thin films, with pore radii much smaller than polymer radii of gyration. Moreover, such composites can be readily produced using the CaRI method and thus the conclusions described in this work can be directly tested experimentally. Our predictions open an exciting space for experimental design of materials with new chemical environments and applications using previously immiscible polymer blends.

■ RESULTS

The HPF⁵⁶ method outlined in the Materials and Methods section is used to simulate binary homopolymer blends confined within a nanoparticle packing. Briefly, the two polymer species are described as discrete Gaussian chains that interact with each other through a Flory potential where the repulsion has a magnitude of χN . In the HPF method, we assume an incompressible system with a constant density ρ_0 ,

and the fields are solved under the mean-field approximation. Nanoparticles are explicitly described as cavity functions that exclude the polymer. The density associated with the nanoparticle changes smoothly from the average density ρ_0 to 0 over a small length scale ξ . We begin with 2D simulations with the nanoparticles fixed on a square lattice so their surfaces contact, and the polymer is only allowed in the pores between the particles. The nanoparticles are immobile, as in the CaRI method for producing dense ternary composites nanoparticles are spin-coated into a jammed, random close-packed film, and there is no evidence of the particle layer expanding or undergoing rearrangement during infiltration. 49,66 The two polymers in the blend have identical interactions with the nanoparticles; neither preferentially wets the surfaces. Experimentally, such a system can be achieved either through the use of two polymers with similar preference for the nanoparticle surface or through functionalization of the nanoparticle surface, such as the silanization of silica nanoparticles. The confinement ratio of this system is defined as $\Gamma = \frac{R_{\rm g}}{R_{\rm pore}}$, where

 $R_{\rm g}$ is the radius of gyration of the polymers and $R_{\rm pore}$ is the pore size of the packing as defined in Figure 1.

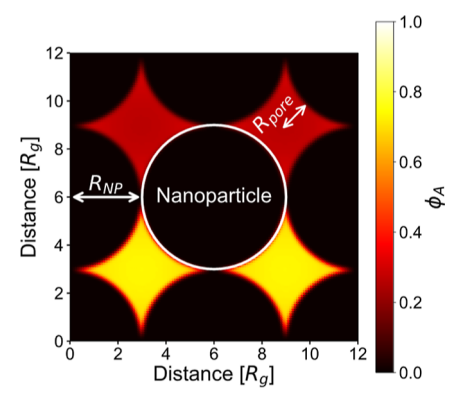


Figure 1. Simulation map output from a HPF SCFT simulation. The x and y axes represent distances along the simulation box in either direction, in units of radius of gyration of the polymers. The nanoparticles are shown in black, with no polymer present within the nanoparticles. The heat map depicts the volume fraction of polymer A, $\phi_{\rm A}(r) = \rho_{\rm A}(r)/\rho_0$, and phase separation can clearly be seen between the top and bottom pores.

We begin by calculating the binodal envelopes of phase diagrams for our system at several values of the Flory–Huggins interaction parameter, χN , which controls repulsion between the two polymers, while changing Γ from 0.8 to 5.1. This range of Γ can be readily prepared experimentally via infiltration of polymers into densely packed nanoparticle packings via CaRI. ⁴⁹ Figure 2a shows a clear trend of increasing miscibility with increasing confinement as larger values of χN are required to enter the two-phase regime at larger Γ . The monotonic increase in the critical point in more confined systems is shown in Figure 2b. The Flory–Huggins interaction parameter is inversely proportional to temperature, and an increase of the bare χ_c value from 0.2 to 0.86 when increasing from a bulk blend to Γ of 5.1 represents an enormous increase in the miscibility window of the blend.

Figure 3 depicts the equilibrium volume fraction of polymer A within the simulation box at each Γ for $\chi N = 5$. According to the calculated binodal phase diagrams, this condition should be within the miscible regime for the two highest Γ sampled. All simulations are initialized such that the A-lean phase localizes to the top two pores and the A-rich phase localizes to the bottom two pores. The average volume fraction within these pores represents the two sides of the binodal curve for that system. A clear transition from phase separation to miscibility is shown between $\Gamma=3.6$ and $\Gamma=4.4$. For $\Gamma=3.6$, a A-rich phase with $\phi_{\rm A} \approx 0.85$ is visible in the bottom two pores and a A-lean phase with $\phi_{\rm A} \approx 0.15$ is visible in the top two pores, consistent with the binodal phase diagram shown in Figure 2a. Under highly confined conditions, we find $\phi_A = 0.5$ in both the top and bottom pores. As the simulations are initialized with $\phi_{\rm A}$ = 0.5, this represents a fully miscible system.

To verify that our predictions are not sensitive to many of the assumptions that enter in the HPF calculations, we perform TILD simulations of binary polymer blends confined to disordered nanoparticle packings. In the TILD method, we can perform 3D simulations of a model that is identical to the HPF model other than the Flory potential is made non-local. The TILD method does not rely on the mean-field approximation and fully samples the thermodynamic fluctuations and the non-local interactions reproduce liquid-like layering near particle surfaces. In contrast to the HPF method, these 3D TILD simulations explicitly track both polymer and NP coordinates using particle representations. Figure 4 shows the potential energy that originates from polymer A/polymer B contacts

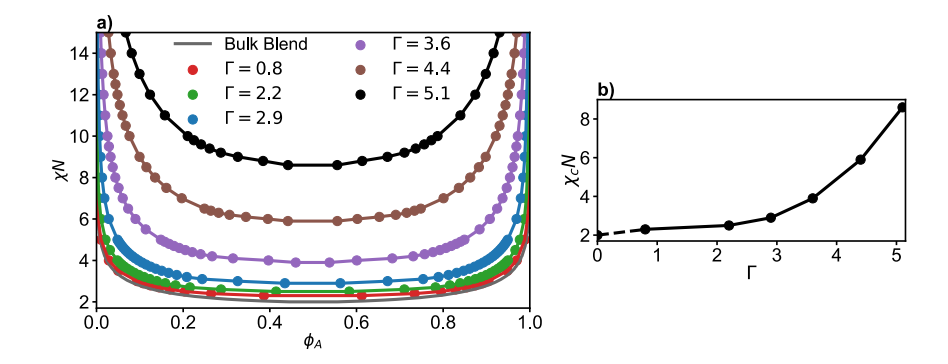


Figure 2. (a) Binodal phase diagrams calculated with the HPF method, plotted as the Flory—Huggins parameter (χN) vs the volume fraction of polymer A within the pore (ϕ_A), for different values of Γ . The binodal for a bulk blend of two symmetric homopolymers ($N_A = N_B = 10$) with no nanoparticles is shown in gray. (b) Critical χN values plotted vs Γ . The critical value is found by systematically increasing χN and finding the value at which the system transitioned from a miscible to a phase-separated state, then fitting the binodal points to an even power series. The bulk critical point (0, 2) is included for reference and is connected to the calculated data with a dashed line.

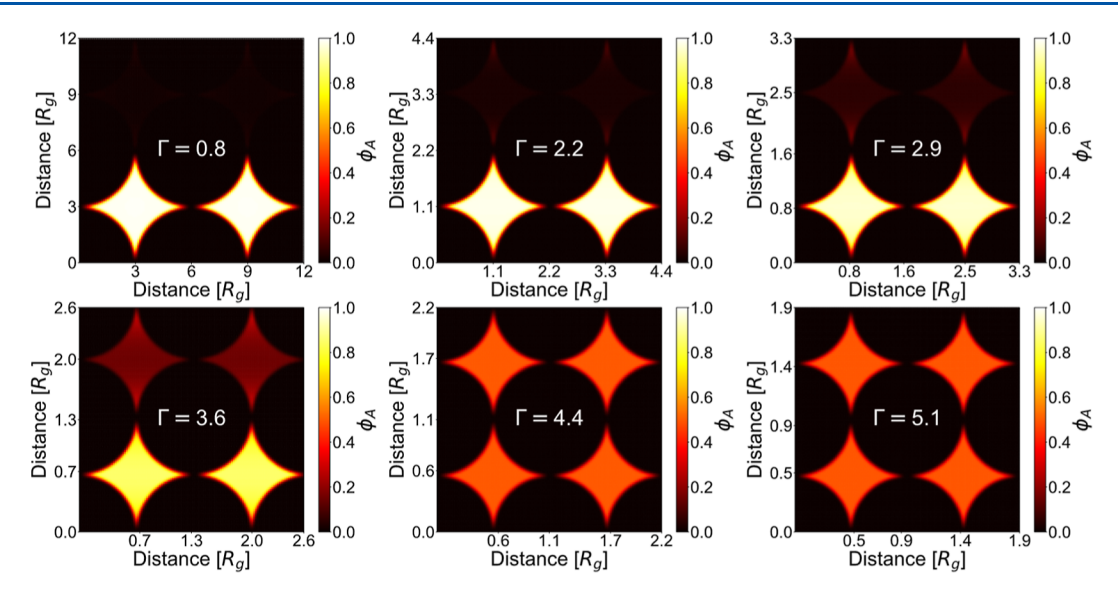


Figure 3. Equilibrium density maps of polymer A at increasing Γ for $\chi N = 5.0$. The heat map depicts the volume fraction of polymer A, ϕ_A , with the upper and lower sets of pores representing the minor and major binodal phases, respectively.

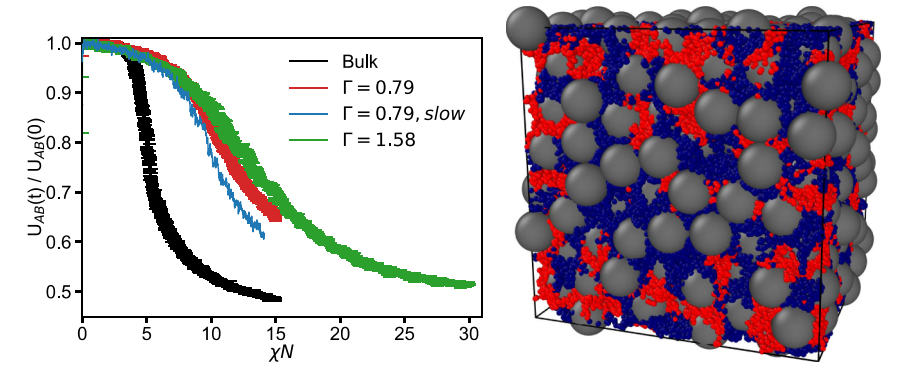


Figure 4. (Left) Relative change of the potential energy between A and B components as χN is increased in a 3D TILD simulation of polymers confined to a random nanoparticle packing. Weak confinement ($\Gamma = 0.79$) shifts the onset of phase separation to significantly higher χN and is modestly sensitive to the rate of change of χN , while stronger confinement ($\Gamma = 1.58$) further increases the transition. (Right) Snapshot of our 3D simulation cell prior to phase separation.

during a simulation that continuously increases χN (see the Supporting Information). The plot labeled "slow" has a rate of increase of χN ten times slower than the other plots to ensure that there is not a large sensitivity to this rate. The inflection point is taken as the onset of phase separation in these systems. The simulations are performed at a dimensionless polymer concentration of C=0.85 ($N\approx175$), corresponding to a strongly fluctuating system, which contributes to the increase of the critical $\chi_c N$ in the bulk system. Upon confinement, the critical χN approximately doubles and continues to increase with increasing confinement, consistent with the 2D HPF results. This verifies that our results do not qualitatively depend on dimensionality or the explicitly fixed uniform nanoparticle packing in the HPF results.

To understand the mechanism of increased miscibility in confined polymer blends, we investigate the enthalpic and entropic contributions to the free energy of mixing for these systems. The derivation of the enthalpy and entropy from HPF simulations is described in the Supporting Information. The values shown in this work are normalized by the interstitial pore volume, $V_{\rm pore} = V_{\rm total} - V_{\rm NP}$, to compare the free energy per unit volume between different values of Γ . Figure 5a shows the change in enthalpy ($\Delta U_{\chi N} = U_{\chi N} - U_{\chi N=0}$) with increasing

 χN for each Γ, with data from simulations plotted as open circles. Prior to phase separation, an increase in χN increases the overall enthalpy of the system, as is visible for all Γ values in Figure 5a. The inset in Figure 5a shows the total change in enthalpy prior to phase separation, or the value of the enthalpy at the critical point, versus Γ, which increases with increasing confinement. Upon phase separation in polymer blends the number of unfavorable A–B contacts is reduced, thus reducing the overall enthalpy of the system. This reduction in enthalpy reduces the free energy of the system making phase separation more energetically favorable. The dashed lines in Figure 5a show the enthalpy predicted by the Flory–Huggins theory, $\frac{\Delta U_{\rm FH}}{V k_{\rm B} T} = \frac{\int {\rm d} \tau \chi N \ \phi(r)(1-\phi(r))}{\int {\rm d} r}$. Prior to and shortly after the critical point of each Γ, the Flory–Huggins theory overpredicts the enthalpy, with this magnitude of overprediction increasing for

Figure 5b shows the change in entropy $(-T\Delta S)$ with increasing χN for each Γ . The entropy of a miscible system remains constant, as observed in the plots for all Γ with a constant value of $-T\Delta S$ for χN below the critical point. Upon phase separation, the entropy of polymer blends decreases, unfavorably increasing the overall free energy of the state. This

increasing Γ .

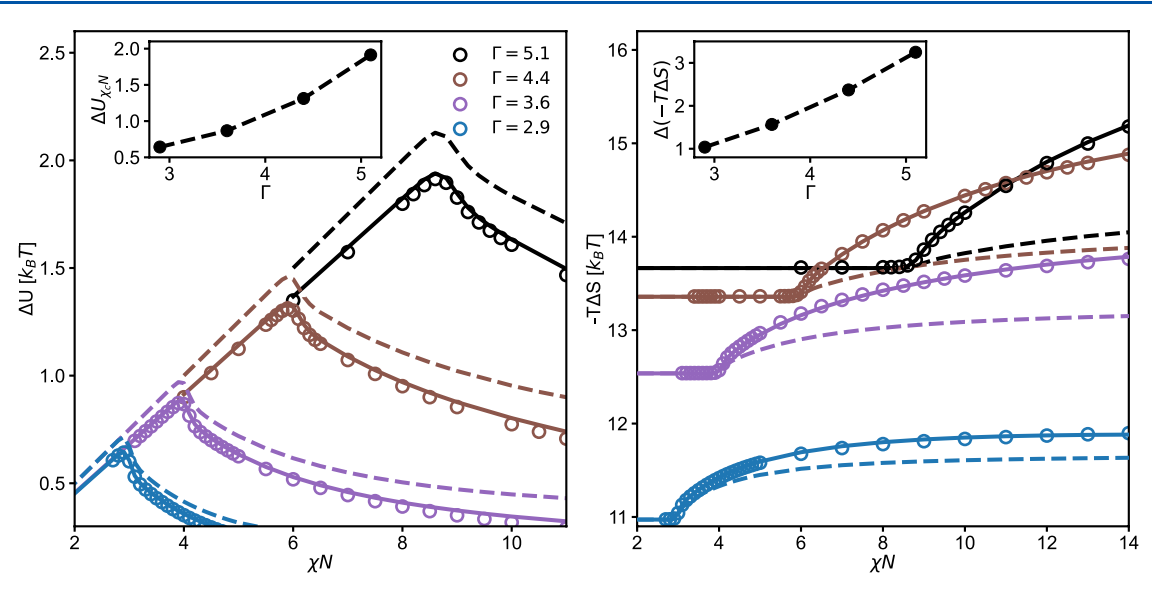


Figure 5. (a) Change in enthalpy vs the Flory–Huggins parameter (χN) for different values of Γ. Data from simulations is plotted with open circles. The dashed lines show the enthalpy predicted by the Flory–Huggins theory, $\frac{\Delta U_{\rm FH}}{Vk_{\rm B}T} = \frac{\int {\rm d}r\chi N\phi(r)(1-\phi(r))}{\int {\rm d}r}$. The solid lines show the enthalpy corrected for surface effects with an effective interaction parameter, $\frac{\Delta U_{\rm eff}}{Vk_{\rm B}T} = \frac{\int {\rm d}r\chi N_{\rm eff}\phi(r)(1-\phi(r))}{\int {\rm d}r}$. The inset plot shows $\Delta U_{\chi_c}N$, the change in enthalpy prior to phase separation, vs Γ. (b) Change in entropy vs the Flory–Huggins parameter (χN) for different values of Γ. Data from simulations is plotted with open circles. The dashed lines show the entropy predicted by the Flory–Huggins theory, $\frac{-T\Delta S_{\rm FH}}{Vk_{\rm B}T} = \frac{\int {\rm d}r\phi(r) \ln \phi(r) + (1-\phi(r)) \ln (1-\phi(r))}{\int {\rm d}r}$. The solid lines show the entropy corrected for changes in conformational entropy near NP surfaces, $\frac{-T\Delta S_{\rm eff}}{Vk_{\rm B}T} = \frac{\int {\rm d}r\phi(r) \ln \phi(r) + (1-\phi(r)) \ln (1-\phi(r))}{\int {\rm d}r}$. The inset plot shows $\Delta(-T\Delta S)$, the change in entropy upon phase separation, or from $\chi N < \chi_c N$ to $\chi N \gg \chi_c N$, vs Γ. In both plots, the change is

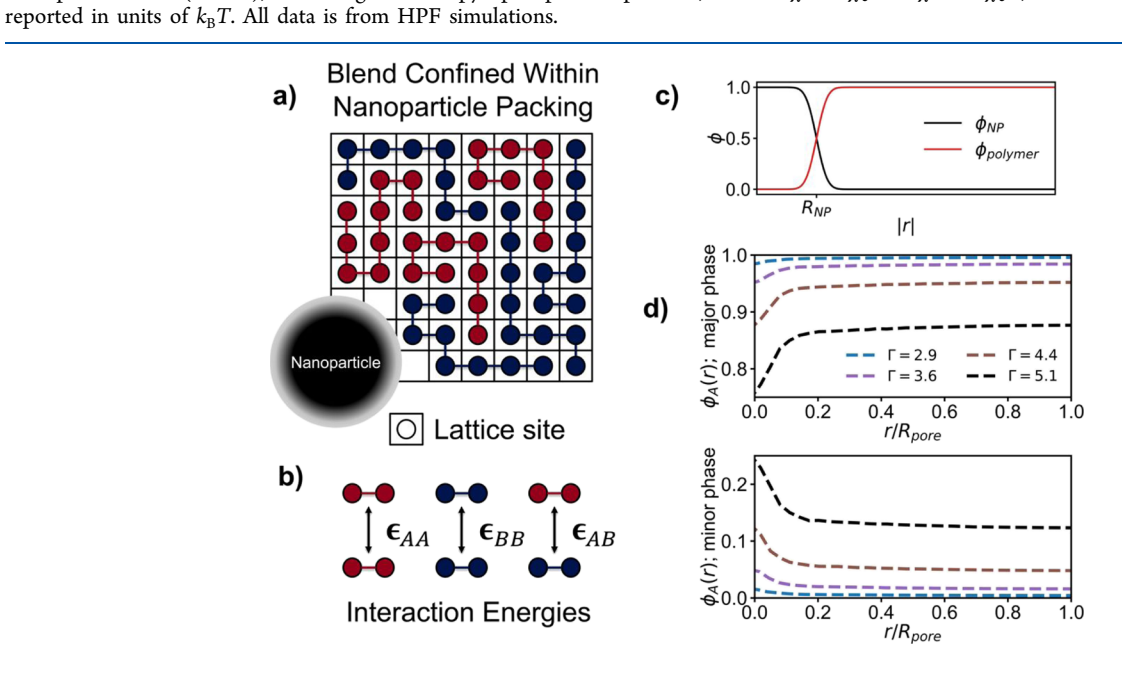


Figure 6. Schematic showing the cause of energetic changes when a polymer blend is confined within a nanoparticle packing. (a) Polymer blend on a lattice in the presence of a nanoparticle. The shading of the nanoparticle displays the decay of nanoparticle density within the surface region. (b) Visualization of the interactions between monomers on a lattice. χN depends on the energies, ϵ , and frequency of these interactions, or the coordination number of the monomers (c) Plot depicting the dependence of the nanoparticle and total polymer volume fractions on distance from the nanoparticle center, |r|. The surface region is defined as the region over which $\phi_{\rm NP}$ decays from 1 to 0. The coordination number of polymers occupying lattice sites within the surface region is lower, reducing the enthalpy. (d) Concentration profile of one polymer vs distance from the nanoparticle surface normalized by the pore radius, $\phi_{\rm K}(r) = \frac{\rho_{\rm K}(r)}{\rho_{\rm A}(r) + \rho_{\rm B}(r)}$. The major phase is shown in the top plot with the corresponding minor phase in the bottom plot. Each color corresponds to a different confinement ratio. The profiles are for $\chi N = 12$, a value at which all systems are phase-separated.

entropic loss must be overcome by a decrease in enthalpy for phase separation to occur. The inset in Figure 5b shows the total change in entropy upon phase separation versus Γ ; the magnitude of entropy decrease upon phase separation increases with increasing confinement. The dashed lines in Figure 5b show the entropy predicted by the Flory–Huggins

theory,
$$\frac{-T\Delta S_{\text{FH}}}{Vk_{\text{B}}T} = \frac{\int \mathrm{d}r\phi(r) \, \ln \phi(r) + (1-\phi(r)) \, \ln \, (1-\phi(r))}{\int \mathrm{d}r}$$
. After the

onset of phase separation, the Flory–Huggins theory underpredicts the value of $-T\Delta S$; the entropy, ΔS , of the systems decreases more than expected for a bulk polymer blend. As shown in both the entropic and enthalpic data, a model beyond the simple bulk Flory–Huggins theory is necessary to explain the thermodynamic behavior of polymer blends confined in dense nanoparticle packings.

The free energy of a polymer blend confined within a nanoparticle packing can be modeled by the equation 67-69

$$\begin{split} \frac{\Delta F}{V k_{\rm B} T} &= \left(\int \mathrm{d}r \left[\chi N_{\rm eff}(r) \phi(r) (1 - \phi(r)) + \phi(r) \, \ln \phi(r) \right. \right. \\ &+ \left. \left. \left(1 - \phi(r) \right) \, \ln (1 - \phi(r)) \right. \\ &+ \left. \frac{a^2}{36 \phi(r) (1 - \phi(r))} \left(\frac{\mathrm{d}\phi(r)}{\mathrm{d}r} \right)^2 \right] \right) \div \int \mathrm{d}r \end{split}$$

where $\chi N_{\rm eff}$ is an effective Flory–Huggins repulsion detailed below and a^2 is the effective lattice parameter. The full derivation of this model is included in the Supporting Information. Unlike similar derivations in thin film systems where polymer concentration varies in only one direction perpendicular to the surfaces, the equilibrium concentration profile, $\phi(r)$, is dependent on both the x and y directions. In a 3D simulation, the concentration profile would be dependent on the x, y, and z dimensions due to the presence of nanoparticle surfaces in all directions.

The first term of the free energy expression is a correction to the Flory—Huggins enthalpy equation,

$$\frac{\Delta U_{\text{eff}}}{V k_{\text{B}} T} = \frac{\int \mathrm{d}r \chi N_{\text{eff}} \phi(r) (1 - \phi(r))}{\int \mathrm{d}r}$$

plotted as solid lines in Figure 5a. Previous work in the thermodynamics of polymer blends under thin film confinement have found a geometric effect of film thickness on the miscibility of the blend, 70,71 which can be captured by an effective interaction parameter, $\chi N_{\rm eff}$, through the Flory-Huggins lattice theory. In polymer blend thermodynamics, it is assumed that the lattice site coordination number is uniform throughout the system and thus the number of segment Asegment B interactions is uniform throughout. As a result, only a single χN value is needed and is defined as $\chi = \frac{Z}{2} \frac{(2\epsilon_{AB} + \epsilon_{AA} + \epsilon_{BB})}{kT}$, where Z is the coordination number of each lattice site and the ϵ terms describe the energy of interactions. Figure 6a shows a polymer blend on a lattice in the presence of a nanoparticle and Figure 6b shows the interactions between monomers on the lattice which are used to define the Flory-Huggins χ . Near nanoparticle surfaces, there exists a region in which the coordination number of lattice sites is reduced due to altered packing of polymers. In HPF simulations, ξ is the length scale over which the nanoparticle volume fraction decays from 1 to 0. This region

is shown schematically in the plot in Figure 6c, and the gradient on the nanoparticle in Figure 6a represents the decay in nanoparticle density. The region defined by ξ is the interfacial width over which the polymers interact with the nanoparticles and thus the area in which polymer lattice sites exhibit reduced coordination number. We define a corrected interaction parameter based on lattice theory such that $\chi N_{\rm eff} = \chi N \times \frac{Z_{\rm s}}{Z}$ where $Z_{\rm s}$ and Z are the coordination numbers of lattice sites in the surface and bulk regions, respectively. $Z_{\rm s}$ is reduced directly by the fraction of lattice sites occupied by nanoparticles, or the volume fraction of nanoparticles. Thus, $\frac{Z_{\rm s}}{Z}$ can be modeled as the total polymer volume fraction at each r, decaying as the red plot in Figure 6c decays.

The final three terms in the free energy equation are entropic in nature. The first two describe the ideal entropy of mixing used in the Flory—Huggins theory, and the third term captures decreased conformational entropy within surface regions near nanoparticles. The solid lines in Figure 5b plot the combination of these terms,

$$\frac{-T\Delta S_{\rm eff}}{Vk_{\rm B}T} = \frac{-T\Delta S_{\rm FH}}{Vk_{\rm B}T} + \frac{\int\!{\rm d}r \frac{a^2}{36\phi(r)(1-\phi(r))} {\left(\frac{{\rm d}\phi(r)}{{\rm d}r}\right)^2}}{\int\!{\rm d}r}$$

Previous work has applied the random phase approximation to model free energy changes of polymer blends at free surfaces 68,72 and walls with asymmetric wetting. 7,69,73 In these studies, differences in interactions between the two polymers and the surface contributed most of the change in free energy, whereas the entropic contribution of the surface was found to be rather small as it scales with the surface area. For a polymer blend at a wall, the surface area of the wall is much smaller than overall volume of the bulk. However, in the extremely confined system we model, the large surface area-to-free volume ratios greatly increase the magnitude of entropic effects.

The scaling of polymer conformational entropy change at an interface with $(\mathrm{d}\phi(r)/\mathrm{d}r)^2$ that has been derived previously⁴³ and arises from changes in the probabilities of different chain orientations near an interface. At a polymer–polymer interface, chains are biased to turn toward the phase of which they are the major component, reducing the total configurations available to each chain in the interfacial region. The length scale a is typically taken as the effective lattice spacing or the statistical segment size, but because previous work has shown that this length scale can change in thin film confinement,⁷⁴ we take a as an adjustable fitting parameter. Further discussion on this parameter is included within the Supporting Information.

Figure 6 shows the concentration profile of one polymer versus distance from the nanoparticle surface normalized by the pore radius, $r/R_{\rm pore}$ at $\chi N=12$, a value at which all systems are phase-separated. The major phase is depleted at the surface, whereas the minor phase is enriched at the surface, and it is this spatial variation that leads to the additional contribution of the entropic term proportional to $({\rm d}\phi/{\rm d}r)^2$. Near the surfaces, the strength of repulsive interactions is reduced. This reduction in enthalpy allows for the system to take on the entropic penalty of an inhomogeneous concentration profile, with the minor phase localizing more toward the surface to reduce contact with unlike polymer in the major phase. Of note is that as the system confinement increases, the length scale over which a gradient is present in

the concentration increases to a larger fraction of the overall pore size. Prior to phase separation no such gradient exists, but upon phase separation a maximum value of the gradient is achieved, explaining the large increase in entropy upon phase separation beyond that predicted by the Flory—Huggins entropy of mixing.

We find that confinement greatly increases the entropic penalty upon phase separation; a larger Γ leads to a larger conformational entropy penalty. The fact that a concentration gradient forms in all directions, and not just in one direction as in thin films, means these gradients create a much larger entropic penalty upon phase separation than seen in previous systems, explaining the large increases in miscibility observed in this work. This entropic penalty is offset by a reduced number of polymer-polymer contacts near surfaces; the increasing surface area with greater confinement further reduces enthalpic penalty near nanoparticles, permitting further enrichment of the minor component near surfaces. The increased miscibility of polymer blends confined within dense nanoparticle packings is thus driven by both a reduction in conformational entropy and a decrease in the strength of enthalpic repulsion near nanoparticle surfaces.

DISCUSSION

In this work, the impact of extreme nanoconfinement within the pores of nanoparticle packings on the thermodynamics of polymer blends is investigated using SCFT and TILD simulations. Confinement strongly increases the miscibility of polymer blends, with an exponential increase in the critical point between regimes where the pore size is equal to the polymer R_g and where the pore size is one-fifth the R_g . The monotonic trend of this increase suggests that further confinement could increase miscibility further, allowing for the preparation of miscible blends from two polymers that would phase-separate in bulk. This change in phase behavior occurs in the presence of neutral surfaces and does not require strong surface interactions like in small-molecule fluids. The free energy of these systems reveals that there is a reduced enthalpic incentive for phase separation in confined systems due to reduced polymer-polymer interactions near nanoparticle surfaces. Future work is necessary to determine how introducing further terms to the enthalpy, such as asymmetric polymer-nanoparticle interactions, would affect the phase behavior. Additionally, the conformational entropy penalty upon phase separation increases with increasing confinement, further driving confined systems toward miscibility. The entropic penalty is much larger than the change in enthalpy with increasing confinement. This makes extreme nanoconfinement-induced miscibility unique from previously described changes in polymer phase behavior between surfaces, which were enthalpically driven. An experimental system which achieves composites with levels of confinement described in this work has previously been developed.^{49,50} These results could be used to design new nanocomposites with unique chemical micro/nano-environments which previously could not be achieved without the use of additives due to their low miscibility.

MATERIALS AND METHODS

Hybrid Particle-Field Method. Binary polymer blends with dense nanoparticle packings are simulated using the HPF method developed previously within an in-house C++ program. In the HPF theory model, explicit nanoparticle positions are retained during the

particle-to-field transformation, and nanoparticle shapes are defined with a cavity function centered at the particle positions. An incompressibility constraint, in tandem with this cavity function, excludes polymers from the volume occupied by the nanoparticles. The HPF method has been used to simulate polymer—nanoparticle mixtures with mobile particles. 56,75 In contrast, this work focuses on simulating the miscibility of two polymers confined in a dense packing of particles akin to those found in polymer infiltrated nanoparticle packings and thus the nanoparticles remain fixed in space. 49,66 Interactions between the polymers are modeled with a Flory—Huggins χ parameter, and there are no interactions between the polymers and the nanoparticle surfaces. This method is described in more detail in the Supporting Information.

Generating Confined Systems. The Γ of this system is defined as $\Gamma = \frac{R_g}{R_{pore}}$, where R_g is the radius of gyration of the polymers and R_{pore} is the pore size of the packing. A 2D simulation box with periodic boundary conditions is used, which has equal lengths in the x and y directions, $L_x = L_y$, unless otherwise stated. For all Γ , N_A , N_B and thus R_g , are held constant. The lengths in the simulation box are nondimensionalized with respect to R_g ; changing R_g without changing the box size or NP radius does not alter the Γ . As shown in Figure 1 of the main text, the simulations contain four fixed-position nanoparticles of equal size: one centered at the origin, one at $0.5 \times L_y$, one at $0.5 \times L_x$, and the final in the center of the box. The box lengths in both directions are set to $4 \times R_{NP}$ so that the NP edges are touching and a 2D packing of nanoparticles and interstices is formed, and we use the diagonal surface-to-surface distance to define R_{pore} (see Figure 1)

Binodal Calculation. To bias our system toward a macrophaseseparated state, we find that using an initial chemical potential field $w_{AB}^{-}(r)$ of a sine wave of amplitude and period 1 in the y-direction and uniform in the x-direction leads to the lowest free energies compared to other biasing approaches. After convergence, in the twophase regime the minority-A phase localizes to the top two pores in the simulation box and the majority A phase localizes to the bottom two pores. All simulations are run at $\phi_{\rm A}$ = 0.5, meaning the volume fractions within the top and bottom pore regimes are the points on the right and left sides of the binodal curve, respectively. Because in this work we only consider symmetric systems with $N_{\rm A}$ = $N_{\rm B}$ and neutral interactions between both polymers and the nanoparticles, we expect our phase envelopes to be symmetric about $\phi_A = 0.5$. The density of each polymer throughout the simulation box at equilibrium is output and averaging over the pore area provides the binodal values, and for select states we have verified that the results of our NVT ensemble simulations give binodal concentrations that agree with those obtained from the μVT ensemble. The μVT ensemble results are shown in Figure S1 of Supporting Information.

Entropy and Potential Energy Analysis. The blends under increasing confinement are analyzed to determine if increased miscibility is driven by entropic or enthalpic effects. The derivation for the expressions used has been derived previously⁷⁶ and begins with the thermodynamic expressions

$$U = T \left(\frac{\partial \log Z}{\partial T} \right)$$

and F = U - TS. As all energies are scaled by kT, we assume that $\chi \propto 1/T$, and taking the partial derivative of the partition function with respect to T gives

$$\Delta U = -\frac{C}{\gamma N} \int \! \mathrm{d}r (\omega_{\mathrm{AB}}^{(+)2}(r) + \omega_{\mathrm{AB}}^{(-)2}(r)) \label{eq:deltaU}$$

where C is the chain density defined as $C = \frac{\rho_0 R_g^3}{N}$. Finally, we calculate the entropy as $-T\Delta S = \Delta F - \Delta U$ and $\Delta F = \Delta H$, where ΔH is the change in the HPF simulation Hamiltonian.

Numerical Methods and Parameters. The propagators for the discrete Gaussian chains in this model are calculated by iterating the Chapman—Kolmogorov equation. This series of convolutions is

efficiently calculated with a series of Fourier transform/inverse Fourier transform pairs using the Fastest Fourier Transform in the West (FFTW) library. The MF approximation used in these simulations permits the assumption that one field configuration $\{\omega^*\}$ dominates the partition function, and we use a first-order semi-implicit method to solve for $\{\omega^*\}$. In all calculations presented in this work, both homopolymer chains have a degree of polymerization N=10, and we have verified that these results agree with those obtained from confined systems with higher N. NVT ensemble phase diagrams for N=100 are shown in Figure S1 of Supporting Information. There are no interactions between the polymers and nanoparticle surfaces beyond the excluded volume enforced by the incompressibility constraint. To ensure gradients at the particle interface do not strongly impact the results, the grid dimensions, N_x and N_w are chosen such that $L_\alpha/N_\alpha \leq \xi$ for $\alpha \in \{x, y\}$.

Theoretically Informed Langevin Dynamics Method. To ensure that our predictions are not sensitive to fluctuation effects, dimensionality, and the geometry of our nanoparticle packing, we perform TILD simulations of a polymer blend both in bulk and in nanoparticle packings. Our TILD simulations use a weakly compressible model, and the mass of a coarse-grained polymer monomer is distributed over a finite volume described by a Gaussian, in contrast to the point-particle model used in the hSCFT calculations. A complete description of the relationship of the standard SCFT methods and TILD simulations can be found in previous work. 79

Our TILD simulations are performed at a polymer concentration of $C \approx 0.85$, which corresponds to low molecular weight polystyrene with $M_{\rm n} \approx 6000$ gm/mol and $R_{\rm g} \approx 2$ nm. The polymer chains are discretized into N = 20 interaction sites, and two nanoparticle sizes are simulated at $R_p = 2.11R_g$ and $4.21R_g$, corresponding to Γ of Γ = $R_{\rm e}/R_{\rm p}$ of 1.58 and 0.79, respectively. Systems are initialized with the nanoparticles randomly distributed through the simulation box, giving a non-uniform distribution in pore size closer to that of an experimental system. The polymer chains are grown as Gaussian random walks beginning from random positions in the box. A sequence of simulations mimicking the "soft push-off" method commonly used to initialize polymer simulations⁸⁰ is employed to eliminate nanoparticle and polymer-particle overlaps where the polymer-particle and particle-particle interaction strength is gradually increased. Simulations to initialize the systems from random configurations are run at least 50 times the polymer diffusion time in the most confined geometry, $\tau = R_g^2/D \approx 1.72$, where D is calculated from the polymer monomer mean-square displacement, and the edge of our cubic simulation cell is approximately $30R_o$. All simulations except for the slowest confined case are run in triplicate, and uncertainties are taken as the standard error of the mean from the three duplicate simulations.

Phase separation is induced through a continuous increase in χN over the course of long simulations. The standard rate of change of χN is 0.0035 per polymer diffusion time, whereas the slow rate is ten times slower. The critical χN value to induce phase separation is obtained by tracking the total potential energy between the A and B monomers, $U_{AB}(t)$ (see Figure 4), and the inflection point in $U_{AB}(t)$ is taken as the critical χN value to induce phase separation in each system.

ASSOCIATED CONTENT

Supporting Information

The Supporting Information is available free of charge at https://pubs.acs.org/doi/10.1021/acs.macromol.2c01918.

Description of HPF and TILD methods, derivation of free energy equation and interaction parameter correcting function, binodal phase diagrams generated in the μVT ensemble, binodal phase diagrams generated inthe NVT ensemble with longer chain length, energy plots and phase diagrams showing impact of changing the

numerical parameter ξ on blend behavior, and discussion of lattice parameter a (PDF)

AUTHOR INFORMATION

Corresponding Authors

Daeyeon Lee — Department of Chemical and Biomolecular Engineering, University of Pennsylvania, Philadelphia, Pennsylvania 19104, United States; orcid.org/0000-0001-6679-290X; Email: daeyeon@seas.upenn.edu

Robert A. Riggleman — Department of Chemical and Biomolecular Engineering, University of Pennsylvania, Philadelphia, Pennsylvania 19104, United States; orcid.org/0000-0002-5434-4787; Email: rrig@seas.upenn.edu

Authors

Anastasia Neuman — Department of Chemical and Biomolecular Engineering, University of Pennsylvania, Philadelphia, Pennsylvania 19104, United States; orcid.org/0000-0002-2315-9546

Shannon Zhang — Department of Chemical and Biomolecular Engineering, University of Pennsylvania, Philadelphia, Pennsylvania 19104, United States

Complete contact information is available at: https://pubs.acs.org/10.1021/acs.macromol.2c01918

Notes

The authors declare no competing financial interest.

ACKNOWLEDGMENTS

This work was supported by the National Science Foundation (NSF) Process Systems, Reaction Engineering, and Molecular Thermodynamics Program (award no. CBET-1933704), Graduate Research Fellowship under grant no. DGE-1845298, and the XSEDE EMPOWER program under NSF grant number ACI-1548562. Computational resources were provided by XSEDE award TG-DMR150034 and CHM210018.

REFERENCES

- (1) Ding, Y.; Feng, W.; Lu, B.; Wang, P.; Wang, G.; Ji, J. PLA-PEG-PLA tri-block copolymers: Effective compatibilizers for promotion of the interfacial structure and mechanical properties of PLA/PBAT blends. *Polymer* **2018**, *146*, 179–187.
- (2) Lyatskaya, Y.; Gersappe, D.; Gross, N. A.; Balazs, A. C. Designing Compatibilizers To Reduce Interfacial Tension in Polymer Blends. *J. Phys. Chem.* **1996**, *100*, 1449–1458.
- (3) Koning, C.; Van Duin, M.; Pagnoulle, C.; Jerome, R. Strategies for compatibilization of polymer blends. *Prog. Polym. Sci.* **1998**, 23, 707–757.
- (4) Yang, X.; Wang, H.; Chen, J.; Fu, Z.; Zhao, X.; Li, Y. Copolymers containing two types of reactive groups: New compatibilizer for immiscible PLLA/PA11 polymer blends. *Polymer* **2019**, *177*, 139–148.
- (5) Gu, L.; Nessim, E. E.; Macosko, C. W. Reactive compatibilization of poly(lactic acid)/polystyrene blends and its application to preparation of hierarchically porous poly(lactic acid). *Polymer* **2018**, 134, 104–116.
- (6) Macosko, C. W.; Jeon, H. K.; Hoye, T. R. Reactions at polymer-polymer interfaces for blend compatibilization. *Prog. Polym. Sci.* **2005**, 30, 939–947.
- (7) Leibler, L. Emulsifying effects of block copolymers in incompatible polymer blends. *Makromol. Chem., Macromol. Symp.* **1988**, *16*, 1–17.

- (8) Chang, K.; Morse, D. C. Diblock Copolymer Surfactants in Immiscible Homopolymer Blends: Swollen Micelles and Interfacial Tension. *Macromolecules* **2006**, *39*, 7746–7756.
- (9) Alkhodairi, H.; Russell, S. T.; Pribyl, J.; Benicewicz, B. C.; Kumar, S. K. Compatibilizing Immiscible Polymer Blends with Sparsely Grafted Nanoparticles. *Macromolecules* **2020**, *53*, 10330–10338.
- (10) Xavier, P.; Rao, P.; Bose, S. Nanoparticle induced miscibility in LCST polymer blends: critically assessing the enthalpic and entropic effects. *Phys. Chem. Chem. Phys.* **2016**, *18*, 47–64.
- (11) Keddie, J. L.; Jones, R. A. L.; Cory, R. A. Size-Dependent Depression of the Glass Transition Temperature in Polymer Films. *Europhys. Lett.* **1994**, *27*, 59–64.
- (12) Wang, H.; Hor, J. L.; Zhang, Y.; Liu, T.; Lee, D.; Fakhraai, Z. Dramatic Increase in Polymer Glass Transition Temperature under Extreme Nanoconfinement in Weakly Interacting Nanoparticle Films. *ACS Nano* **2018**, *12*, 5580–5587.
- (13) Wei, T.; Torkelson, J. M. Molecular Weight Dependence of the Glass Transition Temperature (Tg)-Confinement Effect in Well-Dispersed Poly(2-vinyl pyridine)—Silica Nanocomposites: Comparison of Interfacial Layer Tg and Matrix Tg. *Macromolecules* **2020**, 53, 8725—8736.
- (14) Zhang, H.; Sun, D.-D.; Peng, Y.; Huang, J.-H.; Luo, M.-B. Diffusivity and glass transition of polymer chains in polymer nanocomposites. *Phys. Chem. Chem. Phys.* **2019**, *21*, 23209–23216.
- (15) Bodiguel, H.; Fretigny, C. Reduced Viscosity in Thin Polymer Films. *Phys. Rev. Lett.* **2006**, *97*, 266105.
- (16) Hor, J. L.; Wang, H.; Fakhraai, Z.; Lee, D. Effect of Physical Nanoconfinement on the Viscosity of Unentangled Polymers during Capillary Rise Infiltration. *Macromolecules* **2018**, *51*, 5069–5078.
- (17) Hor, J. L.; Wang, H.; Fakhraai, Z.; Lee, D. Effects of polymernanoparticle interactions on the viscosity of unentangled polymers under extreme nanoconfinement during capillary rise infiltration. *Soft Matter* **2018**, *14*, 2438–2446.
- (18) Das A, N.; Begam, M.; Ibrahim, S.; Chandran, V.; Padmanabhan, M.; Sprung, J. K.; Basu, J. K. Viscosity and fragility of confined polymer nanocomposites: a tale of two interfaces. *Nanoscale* **2019**, *11*, 8546–8553.
- (19) Cangialosi, D.; Boucher, V. M.; Alegría, A.; Colmenero, J. Physical aging in polymers and polymer nanocomposites: recent results and open questions. *Soft Matter* **2013**, *9*, 8619–8630.
- (20) Priestley, R. D.; Rittigstein, P.; Broadbelt, L. J.; Fukao, K.; Torkelson, J. M. Evidence for the molecular-scale origin of the suppression of physical ageing in confined polymer: fluorescence and dielectric spectroscopy studies of polymer-silica nanocomposites. *J. Phys.: Condens. Matter* **2007**, *19*, 205120.
- (21) Rittigstein, P.; Torkelson, J. M. Polymer-nanoparticle interfacial interactions in polymer nanocomposites: Confinement effects on glass transition temperature and suppression of physical aging. *J. Polym. Sci., Part B: Polym. Phys.* **2006**, *44*, 2935–2943.
- (22) Bailey, E. J.; Riggleman, R. A.; Winey, K. I. Polymer Conformations and Diffusion through a Monolayer of Confining Nanoparticles. *Macromolecules* **2020**, *53*, 8171–8180.
- (23) Zhang, T.; Winey, K. I.; Riggleman, R. A. Polymer Conformations and Dynamics under Confinement with Two Length Scales. *Macromolecules* **2019**, *52*, 217–226.
- (24) Chen, Y.-L.; Lin, Y.-H.; Chang, J.-F.; Lin, P. Dynamics and Conformation of Semiflexible Polymers in Strong Quasi-1D and -2D Confinement. *Macromolecules* **2014**, 47, 1199–1205.
- (25) Lin, E. Y.; Frischknecht, A. L.; Riggleman, R. A. Chain and Segmental Dynamics in Polymer-Nanoparticle Composites with High Nanoparticle Loading. *Macromolecules* **2021**, *54*, 5335–5343.
- (26) Steinhaus, A.; Pelras, T.; Chakroun, R.; Gröschel, A. H.; Müllner, M. Self-Assembly of Diblock Molecular Polymer Brushes in the Spherical Confinement of Nanoemulsion Droplets. *Macromol. Rapid Commun.* **2018**, 39, 1800177.
- (27) Shi, A.-C.; Li, B. Self-assembly of diblock copolymers under confinement. *Soft Matter* **2013**, *9*, 1398–1413.

- (28) Shin, J. J.; Kim, E. J.; Ku, K. H.; Lee, Y. J.; Hawker, C. J.; Kim, B. J. 100th Anniversary of Macromolecular Science Viewpoint: Block Copolymer Particles: Tuning Shape, Interfaces, and Morphology. *ACS Macro Lett.* **2020**, *9*, 306–317.
- (29) Yu, C.; Xie, Q.; Bao, Y.; Shan, G.; Pan, P. Crystalline and Spherulitic Morphology of Polymers Crystallized in Confined Systems. *Crystals* **2017**, *7*, 147.
- (30) Dai, X.; Li, H.; Ren, Z.; Russell, T. P.; Yan, S.; Sun, X. Confinement Effects on the Crystallization of Poly(3-hydroxybuty-rate). *Macromolecules* **2018**, *51*, 5732–5741.
- (31) Ok, S.; Vayer, M.; Sinturel, C. A decade of innovation and progress in understanding the morphology and structure of heterogeneous polymers in rigid confinement. *Soft Matter* **2021**, *17*, 7430–7458.
- (32) Binder, K.; Horbach, J.; Vink, R.; De Virgiliis, A. D. Confinement effects on phase behavior of soft matter systems. *Soft Matter* **2008**, *4*, 1555–1568.
- (33) Donley, J. P.; Liu, A. J. Phase behavior of near-critical fluids confined in periodic gels. *Phys. Rev. E* **1997**, *55*, 539–543.
- (34) Braun, E.; Chen, J. J.; Schnell, S. K.; Lin, L.-C.; Reimer, J. A.; Smit, B. Nanoporous Materials Can Tune the Critical Point of a Pure Substance. *Angew. Chem., Int. Ed.* **2015**, *54*, 14349–14352.
- (35) Lee, B. P.; Douglas, J. F.; Glotzer, S. C. Filler-induced composition waves in phase-separating polymer blends. *Phys. Rev. E* **1999**, *60*, 5812–5822.
- (36) Ginzburg, V. V.; Qiu, F.; Paniconi, M.; Peng, G.; Jasnow, D.; Balazs, A. C. Simulation of Hard Particles in a Phase-Separating Binary Mixture. *Phys. Rev. Lett.* **1999**, *82*, 4026–4029.
- (37) Ginzburg, V. V.; Peng, G.; Qiu, F.; Jasnow, D.; Balazs, A. C. Kinetic model of phase separation in binary mixtures with hard mobile impurities. *Phys. Rev. E* **1999**, *60*, 4352–4359.
- (38) Balazs, A. C.; Ginzburg, V. V.; Qiu, F.; Peng, G.; Jasnow, D. Multi-Scale Model for Binary Mixtures Containing Nanoscopic Particles. *J. Phys. Chem. B* **2000**, *104*, 3411–3422.
- (39) Araki, T.; Tanaka, H. Wetting-induced depletion interaction between particles in a phase-separating liquid mixture. *Phys. Rev. E* **2006**, 73, 061506.
- (40) Laradji, M.; MacNevin, G. Phase separation dynamics in binary fluids containing quenched or mobile filler particles. *J. Chem. Phys.* **2003**, *119*, 2275–2283.
- (41) Tanaka, H.; Lovinger, A. J.; Davis, D. D. Pattern evolution caused by dynamic coupling between wetting and phase separation in binary liquid mixture containing glass particles. *Phys. Rev. Lett.* **1994**, 72, 2581–2584.
- (42) Taguet, A.; Cassagnau, P.; Lopez-Cuesta, J.-M. Structuration, selective dispersion and compatibilizing effect of (nano)fillers in polymer blends. *Prog. Polym. Sci.* **2014**, *39*, 1526–1563.
- (43) Szleifer, I.; Widom, B. Structure and tension of the interface between dilute polymer solutions. *J. Chem. Phys.* **1989**, *90*, 7524–7534.
- (44) Binder, K. Collective diffusion, nucleation, and spinodal decomposition in polymer mixtures. *J. Chem. Phys.* **1983**, *79*, 6387–6409.
- (45) Laradji, M.; Hore, M. J. A. Nanospheres in phase-separating multicomponent fluids: A three-dimensional dissipative particle dynamics simulation. *J. Chem. Phys.* **2004**, *121*, 10641–10647.
- (46) He, G.; Ginzburg, V. V.; Balazs, A. C. Determining the phase behavior of nanoparticle-filled binary blends. *J. Polym. Sci., Part B: Polym. Phys.* **2006**, *44*, 2389–2403.
- (47) Otero-Navas, I.; Arjmand, M.; Sundararaj, U. Carbon nanotube induced double percolation in polymer blends: Morphology, rheology and broadband dielectric properties. *Polymer* **2017**, *114*, 122–134.
- (48) Nunes, M. A. B. S.; Matos, B. R.; Silva, G. G.; Ito, E. N.; Melo, T. J. A.; Fechine, G. J. M. Hybrids nanocomposites based on a polymer blend (linear low-density polyethylene/poly(ethylene-comethyl acrylate) and carbonaceous fillers (graphene and carbon nanotube). *Polym. Compos.* **2021**, *42*, 661–677.
- (49) Huang, Y.-R.; Jiang, Y.; Hor, J. L.; Gupta, R.; Zhang, L.; Stebe, K. J.; Feng, G.; Turner, K. T.; Lee, D. Polymer nanocomposite films

with extremely high nanoparticle loadings via capillary rise infiltration (CaRI). *Nanoscale* **2015**, *7*, 798–805.

- (50) Venkatesh, R. B.; Manohar, N.; Qiang, Y.; Wang, H.; Tran, H. H.; Kim, B. Q.; Neuman, A.; Ren, T.; Fakhraai, Z.; Riggleman, R. A.; Stebe, K. J.; Turner, K.; Lee, D. Polymer-Infiltrated Nanoparticle Films Using Capillarity-Based Techniques: Toward Multifunctional Coatings and Membranes. *Annu. Rev. Chem. Biomol. Eng.* **2021**, *12*, 411–437.
- (51) Bradford, P. D.; Wang, X.; Zhao, H.; Maria, J.-P.; Jia, Q.; Zhu, Y. T. A novel approach to fabricate high volume fraction nanocomposites with long aligned carbon nanotubes. *Compos. Sci. Technol.* **2010**, *70*, 1980–1985.
- (52) Wu, Y.; Ye, K.; Liu, Z.; Wang, M.; Chee, K. W. A.; Lin, C.-T.; Jiang, N.; Yu, J. Effective thermal transport highway construction within dielectric polymer composites via a vacuum-assisted infiltration method. J. Mater. Chem. C 2018, 6, 6494–6501.
- (53) Alshammary, B.; Walsh, F. C.; Herrasti, P.; Ponce de Leon, C. Electrodeposited conductive polymers for controlled drug release: polypyrrole. *J. Solid State Electrochem.* **2016**, *20*, 839–859.
- (54) Nejati, S.; Lau, K. K. S. Pore Filling of Nanostructured Electrodes in Dye Sensitized Solar Cells by Initiated Chemical Vapor Deposition. *Nano Lett.* **2011**, *11*, 419–423.
- (55) Qiang, Y.; Manohar, N.; Stebe, K. J.; Lee, D. Polymer blend-filled nanoparticle films via monomer-driven infiltration of polymer and photopolymerization. *Mol. Syst. Des. Eng.* **2018**, *3*, 96–102.
- (56) Sides, S. W.; Kim, B. J.; Kramer, E. J.; Fredrickson, G. H. Hybrid Particle-Field Simulations of Polymer Nanocomposites. *Phys. Rev. Lett.* **2006**, *96*, 250601.
- (57) Koski, J. P.; Chao, H.; Tabedzki, C.; Riggleman, R. A.Coarse-Grained Modeling of Polymer Nanocomposites: Field-Theoretic Simulations. In *Theory and Modeling of Polymer Nanocomposites*; Ginzburg, V. V., Hall, L. M., Eds.; Springer Series in Materials Science, 2021; pp 45–79.
- (58) Chao, H.; Koski, J.; Riggleman, R. A. Solvent vapor annealing in block copolymer nanocomposite films: a dynamic mean field approach. *Soft Matter* **2016**, *13*, 239–249.
- (59) Fredrickson, G. H.The Equilibrium Theory of Inhomogeneous Polymers; International Series of Monographs on Physics; Oxford University Press: Oxford, New York, 2006.
- (60) Koski, J.; Chao, H.; Riggleman, R. A. Field theoretic simulations of polymer nanocomposites. *J. Chem. Phys.* **2013**, *139*, 244911.
- (61) Thompson, R. B.; Ginzburg, V. V.; Matsen, M. W.; Balazs, A. C. Predicting the Mesophases of Copolymer-Nanoparticle Composites. *Science* **2001**, 292, 2469–2472.
- (62) Cherrabi, R.; Saout-Elhak, A.; Benhamou, M.; Daoud, M. Phase separation in confined polymer blends. *J. Chem. Phys.* **1999**, *111*, 8174–8181.
- (63) Tang, H.; Szleifer, I.; Kumar, S. K. Critical temperature shifts in thin polymer blend films. *J. Chem. Phys.* **1994**, *100*, *5367*–*5371*.
- (64) Binder, K.; Evans, R.; Landau, D. P.; Ferrenberg, A. M. Interface localization transition in Ising films with competing walls: Ginzburg criterion and crossover scaling. *Phys. Rev. E* **1996**, 53, 5023–5034.
- (65) Jerry, R. A.; Bruce Nauman, E. Phase transitions in thin films of a binary mixture. *Phys. Lett. A* **1992**, *167*, 198–204.
- (66) Shavit, A.; Riggleman, R. A. The dynamics of unentangled polymers during capillary rise infiltration into a nanoparticle packing. *Soft Matter* **2015**, *11*, 8285–8295.
- (67) Schmidt, I.; Binder, K. Model calculations for wetting transitions in polymer mixtures. *J. Phys.* **1985**, 46, 1631–1644.
- (68) Cifra, P.; Bruder, F.; Brenn, R. Surface segregation in a polymer blend. Comparison between Monte Carlo simulation and mean-field theory. *J. Chem. Phys.* **1993**, *99*, 4121–4127.
- (69) de Gennes, P. G.; Witten, T. A. Scaling Concepts in Polymer Physics. *Phys. Today* **1980**, *33*, 51–54.
- (70) Pan, Q.; Composto, R. J. Phase Separation Studies of Confined Thin Film Polymer Blends. *Mater. Res. Soc. Symp. Proc.* **1994**, 366, 27.

- (71) Reich, S.; Cohen, Y. Phase separation of polymer blends in thin films. J. Polym. Sci., Polym. Phys. Ed. 1981, 19, 1255–1267.
- (72) Forrey, C.; Koberstein, J. T.; Pan, D. H. Surface Segregation in Miscible Blends of Polystyrene and Poly(vinylmethyl ether): Comparison of Theory and Experiment. *Interface Sci.* **2003**, *11*, 211–223.
- (73) Saout-Elhak, A.; Benhamou, M.; Daoud, M. Phase Separation in Polymer Blends Near a Surface. *J. Phys. II* **1997**, *7*, 503–516.
- (74) Cavallo, A.; Müller, M.; Binder, K. Unmixing of Polymer Blends Confined in Ultrathin Films: Crossover between Two-Dimensional and Three-Dimensional Behavior. *J. Phys. Chem. B* **2005**, *109*, 6544–6552.
- (75) Tang, Q.; Ma, Y. Self-Assembly of Rod-Shaped Particles in Diblock-Copolymer Templates. *J. Phys. Chem. B* **2009**, *113*, 10117–10120.
- (76) Lindsay, B. J.; Composto, R. J.; Riggleman, R. A. Equilibrium Field Theoretic Study of Nanoparticle Interactions in Diblock Copolymer Melts. *J. Phys. Chem. B* **2019**, *123*, 9466–9480.
- (77) Frigo, M.; Johnson, S. G.FFTW: an adaptive software architecture for the FFT. *Proceedings of the 1998 IEEE International Conference on Acoustics, Speech and Signal Processing.* ICASSP '98 (Cat. No.98CH36181), 1998; Vol. 3, pp 1381–1384.
- (78) Ceniceros, H. D.; Fredrickson, G. H. Numerical Solution of Polymer Self-Consistent Field Theory. *Multiscale Model. Simul.* **2004**, *2*, 452–474.
- (79) Ginzburg, V. V.; Hall, L. M.Theory and Modeling of Polymer Nanocomposites; Springer Nature, 2020.
- (80) Sliozberg, Y. R.; Andzelm, J. W. Fast protocol for equilibration of entangled and branched polymer chains. *Chem. Phys. Lett.* **2012**, 523, 139–143.

□ Recommended by ACS

Associating Polymers in the Strong Interaction Regime: Validation of the Bond Lifetime Renormalization Model

Sirui Ge, Alexei P. Sokolov, et al.

MARCH 10, 2023

MACROMOLECULES

READ 🗹

Combined Mixing and Dynamical Origins of $T_{\rm g}$ Alterations Near Polymer-Polymer Interfaces

Asieh Ghanekarade and David S. Simmons

DECEMBER 30, 2022

MACROMOLECULES

READ 🗹

Vitrification of the Entire Amorphous Phase during Crystallization of Poly(butylene terephthalate) near the Glass-Transition Temperature

Akihiko Toda, Christoph Schick, et al.

APRIL 14, 2023

MACROMOLECULES

READ 🗹

Rheological Role of Stiff Nanorings on Concurrently Strengthening and Toughening Polymer Nanocomposites

Yu-Chao Li, Xue-Zheng Cao, et al.

JANUARY 24, 2023

ACS MACRO LETTERS

READ 🗹

Get More Suggestions >